

# A deep learning based ABP waveform estimation method using wrist PPG signals

Moustafa Mahmoud *s2422093*

January 28, 2024

<b>Contents</b>		
<b>1 Abstract</b>	<b>2</b>	<b>15</b>
<b>2 Introduction &amp; Background</b>	<b>2</b>	
2.1 Cardiovascular diseases & Hypertension . . . . .	2	
2.2 BP Measurement Methods . . . . .	2	
2.2.1 Sphygmomanometers (Non-Invasive)	2	
2.2.2 Intra-Arterial Cannulation (Invasive)	3	
2.3 ABP Waveform . . . . .	3	
2.4 Photoplethysmography (PPG) . . . . .	3	
2.4.1 Core Principles . . . . .	3	
2.4.2 Recent Advances & Market Adoption	4	
2.4.3 Challenges . . . . .	4	
2.5 PPG for ABP Estimation . . . . .	5	
2.5.1 Deep Neural Networks . . . . .	5	
2.5.2 MIMIC III . . . . .	6	
2.6 Gap in Literatures . . . . .	6	
<b>3 Methodology</b>	<b>7</b>	
3.1 System Overview . . . . .	7	
3.2 Experimental Design . . . . .	7	
3.2.1 Ethical Approval . . . . .	7	
3.2.2 Protocol . . . . .	7	
3.2.3 Equipment . . . . .	8	
3.3 Neural Network Model . . . . .	8	
3.4 Preprocessing . . . . .	8	
3.4.1 Sample Rate Conversion . . . . .	8	
3.4.2 Bandpass Filter: ChebyshevII . . . . .	9	
3.4.3 Segmentation & Normalization . . . . .	9	
3.4.4 Signal Quality Assessment . . . . .	9	
<b>4 Results</b>	<b>10</b>	
4.1 Model Setup . . . . .	10	
4.2 Pre-Processing . . . . .	11	
4.3 Experimental Data Analysis . . . . .	11	
4.3.1 Static [A1 & A3] . . . . .	11	
4.3.2 Dynamic [A2 & A4] . . . . .	12	
4.3.3 SQA . . . . .	13	
4.4 ABP Output . . . . .	13	
<b>5 Discussion</b>	<b>14</b>	
5.1 E4 & PPG Signal Quality . . . . .	14	
5.2 Segment Quality Assessment . . . . .	14	
5.3 System Design . . . . .	15	
<b>6 Conclusions</b>		<b>15</b>
<b>7 Acknowledgements</b>		<b>16</b>

# 1 Abstract

The advances in Machine Learning (ML) models widened the capabilities of biomedical signal processing. One application of ML that garnered recent interest is the estimation of physiological parameters using Deep Neural Networks (DNN). With Cardiovascular Diseases (CVD) posing a global health, recent literature has explored the utility of Deep Neural Networks in estimating Arterial Blood Pressure (ABP) waveforms using Biosignals such as Photoplethysmography (PPG). PPG's advantage is that it is portable and noninvasive, however, it is heavily influenced by motion artifacts (MA).

In this report, the common themes in this avenue of literature will be explored. The advantages and disadvantages of using DNN will be analyzed. From these findings, a DNN model that estimates ABP waveforms from PPG signals will be implemented and evaluated. The data that the system will be tested with are acquired from an experimental protocol that includes static and dynamic activities. The dynamic activities are included as most of the proposed ABP models in the literature are trained on ABP and PPG data from the MIMIC III biosignals database which contains data from ICU patients exclusively.

A preprocessing pipeline will be designed to prepare the PPG segments, followed by a signal quality assessment algorithm that classifies PPG segments into high and low quality, using the Short-Time Fourier Transform (STFT). The high-quality segments will be used as inputs to the model which does 1-to-1 regression from PPG segments to ABP waveform segments.

From the acquired segments during static activities 64.55% & 56.16% for participants 1 and 2 of the protocol. However, none of the segments acquired during the dynamic activities passed the signal quality assessment. Finally, The model outputs ABP waveforms with valid morphological features when the input segments are composed of consistent high-quality PPG pulse waves.

## 2 Introduction & Background

### 2.1 Cardiovascular diseases & Hypertension

Noncommunicable diseases (NCDs) are a global health crisis, accounting for 71% of all deaths. Cardiovascular diseases (CVDs) in particular are the leading cause of morbidity and mortality caused by NCDs, with about 17.9 million lives lost each year due to CVDs [1]. An imperative biomarker for the diagnosis and management of CVDs is blood pressure which is measured during intermittent medical check-ups [2].

Hypertension (HTN) is attributed with the strongest risk factor of CVDs and it affects approximately 1.13 billion people globally. [3].

HTN is the elevation of outward pressure exerted by the circulating blood on the arteries' inner walls, causing excessive strain on the cardiovascular system. Several factors contribute to the exacerbation of HTN including aging, family history, obesity, inactivity, tobacco use, high sodium diets, and stress [4].

The diagnosis of HTN is done by measuring the Systolic (SBP) and Diastolic (DBP) Blood Pressure of the patient and inferring the type of HTN based on the range in which both values lie. The stages of HTN and their ranges can be found in table 1.

Table 1: Blood Pressure Ranges and Associated Conditions [5]

Condition	Systolic (mm Hg)	Diastolic (mm Hg)
Normal	Less than 120	Less than 80
Elevated	120-129	Less than 80
HTN Stage 1	130-139	80-89
HTN Stage 2	At least 140	At least 90
HTN Crisis	Over 180	Over 120

### 2.2 BP Measurement Methods

One categorization of BP measurement methods is invasiveness. Before introducing photoplethysmography, the method used in this assignment, the "golden standard" invasive and non-invasive methods will be briefly introduced, as well as their use cases, pros, and cons.

#### 2.2.1 Sphygmomanometers (Non-Invasive)

Cuff-based sphygmomanometer is a non-invasive BP measurement technique. Sphygmomanometers are regarded as the "golden standard" for in- and out-of-office BP measurement. This method is widely used in medical testing due to its high accuracy, minimal cost, ease of use, and most importantly its noninvasiveness [6].

Sphygmomanometers suffice in terms of diagnostic utility for CVDs that only require SBP and DBP readings. However, these devices measure the SBP and DBP discrete values only.

In Figure 1, the working principle of a digital (Oscillographic) sphygmomanometer can be seen. The device in Fig 1 measures SBP of 120 mmHg over DBP of 80 mmHg, which corresponds to the maximum and minimum Arterial BP (ABP) values. As can be seen in 1(a), ABP fluctuates quasi-periodically with every cardiac signal.

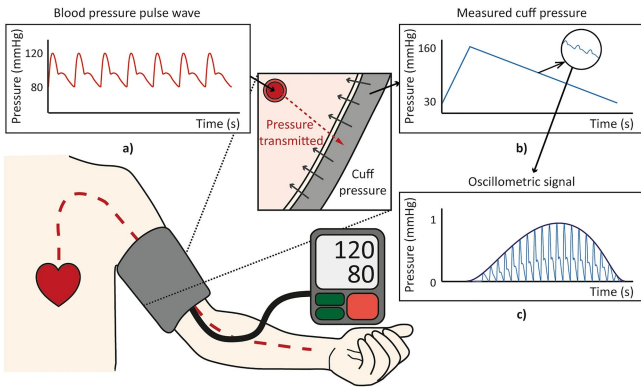


Figure 1: Oscillometric sphygmomanometer: a) BP waveform, b) Cuff pressure measured, c) Oscillometric signal [7]

### 2.2.2 Intra-Arterial Cannulation (Invasive)

This method works by connecting an intra-arterial cannula to a pressure transducer system that converts the fluctuating intra-arterial BP to an electrical signal, displayed as a real-time waveform. The method's working principle can be seen in Figure 2

Invasive cannulation is the most accurate continuous ABP measurement method as it directly interfaces with the arteries with minimal external influences on its reading. However, Cannulation is reserved for use in critical care patients during invasive surgery or in the ICU. A patient has to be anesthetized prior to the insertion of the cannula and the transducer has to be leveled based on the patient's resting position for accurate pressure referencing [8].

The invasiveness of the method, not only comes at the cost of comfort and ease of use but also the risk of serious complications, such as thrombosis, hemorrhaging, arterial injury, and infection [8] [9].

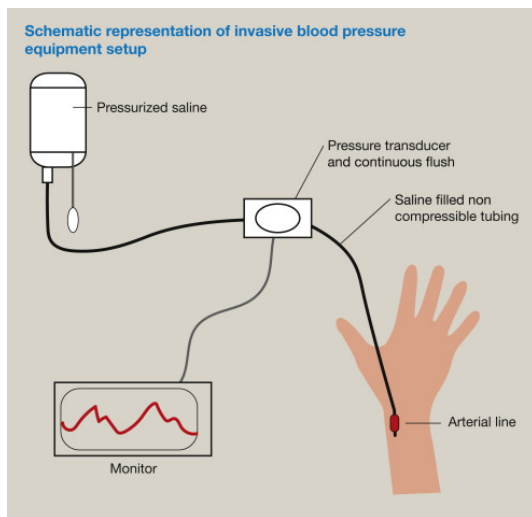


Figure 2: Diagram: Invasive Intra-Arterial Cannulation for ABP measurement [8]

## 2.3 ABP Waveform

Between the SBP and DBP values, ABP fluctuates continuously forming a pulse wave. The ABP waveform provides more complete information about hemodynamic stability and cardiovascular health.

Several features of the ABP pulse wave, seen in Figure 3, are used to characterize and monitor cardiovascular insufficiencies in pertinent CV properties such as cardiac output, vascular resistance, and left ventricle stroke volume [10] [11] [12].

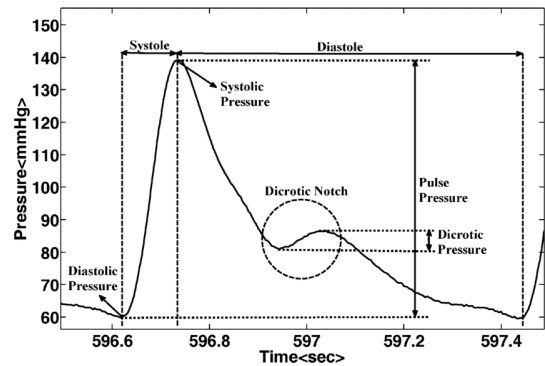


Figure 3: Example of BP Pulse Wave Features [13]

## 2.4 Photoplethysmography (PPG)

### 2.4.1 Core Principles

PPG is a non-invasive optical technique for monitoring changes in arterial blood volume over time, most commonly used in pulse oximeters to measure blood oxygen saturation. The blood is pumped through arteries, carrying oxygenated hemoglobin in red blood cells. Oxygenated hemoglobin highly absorbs most wavelengths of light except for red wavelength light.

By illuminating red light on a skin segment that an artery runs under, and then detecting the absorption/reflection of that light using a photodiode, PPG signals are generated. High red wavelength light detection indicates high oxygen saturation in the blood (SpO<sub>2</sub>) [14].

A diagram demonstrating a PPG pulse wave components can be seen in Figure 4

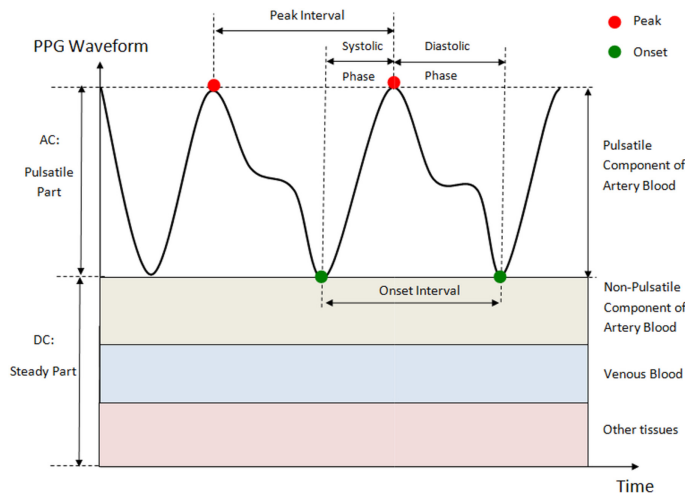


Figure 4: PPG Signal Components/ Features [15]

### 2.4.2 Recent Advances & Market Adoption

The bulk of scientific literature on PPG’s use in ABP estimation was found in the past decade, with the research output accelerating yearly. A paradigm shift towards medical wearables accompanied by advances in PPG sensor design, signal processing, and reduction in hardware costs widened this avenue of research [16].

The global PPG biosensors market is projected to reach USD 839.3 million by 2028 [17]. Most smartwatches on the market house a PPG sensor, mainly for Heart Rate Monitoring (HRM) which is done by measuring the time interval between consecutive PPG systolic peaks.

Recent literature also explored PPG’s utility in detecting arterial stiffness, atrial fibrillation, respiratory rate, and even stress levels [18] [19] [20] [21] [22].

A histogram of the number of publications with the word ”Photoplethysmography” can be seen in Figure 5

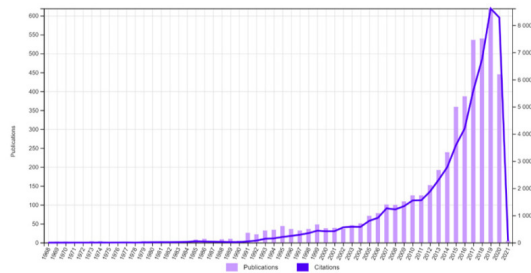


Figure 5: Histogram of the number of publications with the word ”Photoplethysmography” [22]

### 2.4.3 Challenges

Motion Artifacts (MA) are the main source of PPG signals’ contamination. Several solutions were proposed to circumvent this problem with moderate success, but

none eliminated it completely [23] [24] [25] [26] [27].

The mean absolute error (MAE) of HRM using PPG was found to increase by 30%, on average, during movement relative to the accuracy during resting conditions. This is despite the fact that HRM only requires accuracy in the time locality of the systolic peak intervals, as seen in Figure 4. As the peak of the signal should be the strongest component of the signal; Other more nuanced features, both statistically and morphologically, are likely to be even more prone to MA.

In some devices, PPG may also be sensitive to variability in the user’s skin color, body hair density, and skin density [28].

A visual representation of the sources of PPG signal contamination can be seen in Figure 6

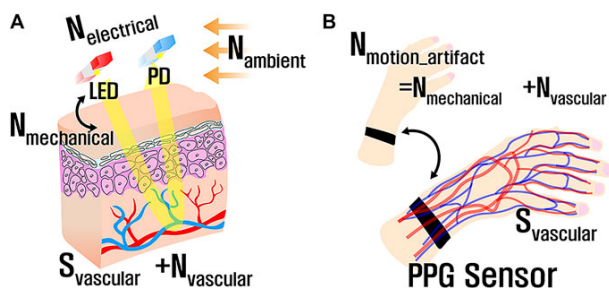


Figure 6: Sources of PPG signal noise [25]

To complicate the problem, inter-variability in cardiovascular & biological parameters can influence PPG features [29]. Modern devices employ PPG arrays that emit light with different wavelengths to improve Signal to Noise Ratio (SNR), allowing the light to penetrate to ranging depths within the tissue [30]. However, high-end PPG sensors are less market-adopted as the salient usage of PPG is to estimate HR and SpO2, both of which do not require high-accuracy signal acquisition. HRM on average was found to only require 5 Hz sampling rate in healthy subjects [31].

Sensing
Sensor geometry
Emitted light intensity
Sensor-skin interface
Photodiode sensitivity
Biological
Oxygen concentration
Organ characteristics
Microcirculation volume
Cardiovascular
Arterial blood volume
Interstitial fluids
Venous volume

Table 2: Other influential factors to PPG [29]

## 2.5 PPG for ABP Estimation

PPG 4 and ABP 3 pulse waves are highly correlated [32]. A large body of literature has explored PPG’s utility for ABP estimation using morphological and statistical features extracted from the PPG data. A common theme in these models is combining Electrocardiogram (ECG) in conjunction with PPG to obtain a more accurate abstraction of the CV system [33] [34] [20].

The highest correlating PPG - ECG feature to ABP is pulse amplitude time (PAT), seen in Figure 10. PAT directly correlates with arterial stiffness which in turn highly correlates with ABP.

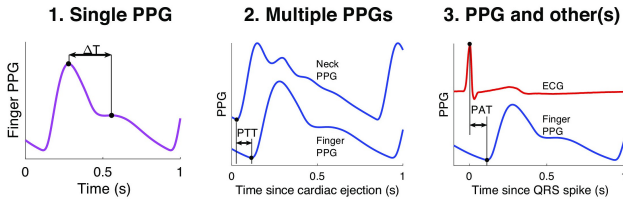


Figure 7: Three common modalities used to predict ABP using PPG [35]

Multi-site PPG from different sensing sights is also used for the same purpose. However, The higher accuracy of multi-modal and multi-channel inputs comes at the cost of mobility and ease of use as ECG is not commonly integrated into daily smart wearables; So daily monitoring will require specialized devices [35].

There are pulse oximeter BP monitoring devices on the market; all of which estimate SBP & DBP discrete values only, which suffices for out-of-office monitoring of HTN. However, HTN is not the only CV phenomenon that is monitored through ABP information. As stated earlier, several physiological parameters can be estimated using ABP waveform features. This leaves room for a broader range of out-of-office diagnostic applications in which ABP waveform features play a significant role.

### 2.5.1 Deep Neural Networks

Researchers have developed highly accurate ABP waveform estimation models with exclusively PPG inputs using Deep Neural Networks (DNN) with several architectures [36] [37] [38] [39] [40]. DNN expanded the capabilities of this type of continuous signal prediction.

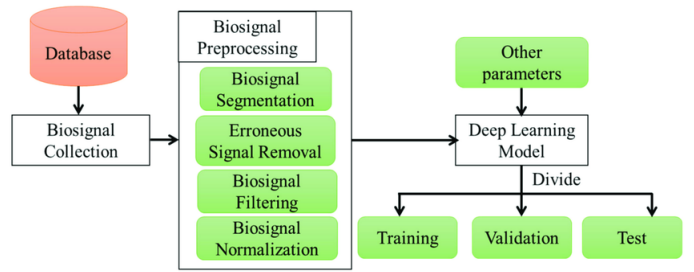


Figure 8: Commonly Used System Design for DNN Predicting Physiological Properties [41]

DNN models are trained to predict continuous waveforms based on the difference between their output data and ground truth data. PPG signals are used as input to the DNN and the output is a result of a series of algebraic computations. The error resultant backpropagates to adjust the values of the variables of the DNN so that the next prediction is closer to ground truth. As this process is repeated iteratively over a large sum of data, the weights of the DNN converge towards values that best predict the ground truth label.

Unlike basic linear regression models, DNNs find non-linear relationships between input and outputs implicitly. The weights between the input nodes, hidden layer nodes, and output nodes create an abstract model that predicts the output based on the stimulus at the input. The training data shapes this model to predict ABP waveform samples at the output in a specific input feature space. When the input feature space shifts the training data space, the model’s abstraction does not always hold up. This underscores the importance of using a diverse set of training data in terms of all relevant variables to the specific use of said model [42].

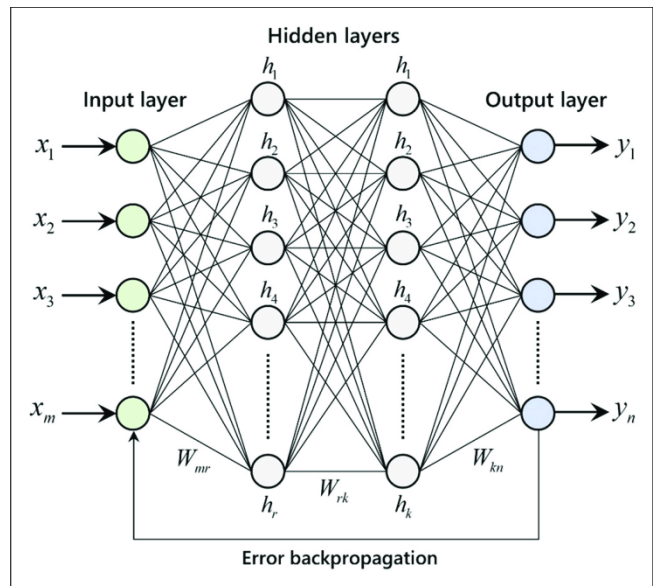


Figure 9: Example of DNN [42]

While several publications developed DNN models with relatively high estimation accuracy, most of these results are only achieved on testing data that is a subset of the same database that the training data was acquired from. Only one publicly available database of time-synchronized PPG & ABP, or subsets of it, is used to train DNN for ABP estimation in most publications. This can be seen in Figure 10.

Database	Source of data	# of subjects	Physiological signals	Demographic information
PulseDB	MIMIC-III matched subset, VitalDB	5,361	ECG, PPG, ABP	Age, Gender, Height <sup>a</sup> , Weight <sup>a</sup> , BMI <sup>a</sup>
Cuff-Less Blood Pressure Estimation Data Set (UCI)	MIMIC-II	~5	ECG, PPG, ABP	-
BP-Net	MIMIC, MIMIC-II	293	ECG, PPG, SBP, DBP	-
MIMIC-II waveform database matched subset v3.1	MIMIC-II	2,809	ECG, PPG <sup>a</sup> , ABP <sup>a</sup> , RES <sup>a</sup> , Others <sup>a</sup>	Age, Gender
MIMIC-III waveform database matched subset v1.0	MIMIC-III	10,282	ECG, PPG <sup>a</sup> , ABP <sup>a</sup> , RES <sup>a</sup> , Others <sup>a</sup>	Age, Gender
MIMIC database v1.0	ICU patients	~90	ECG, PPG <sup>a</sup> , ABP <sup>a</sup> , RES <sup>a</sup> , Others <sup>a</sup>	-
MIMIC-II waveform database v3.2	ICU patients	-	ECG, PPG <sup>a</sup> , ABP <sup>a</sup> , RES <sup>a</sup> , Others <sup>a</sup>	-
MIMIC-III waveform database v1.0	ICU patients	~30,000	ECG, PPG <sup>a</sup> , ABP <sup>a</sup> , RES <sup>a</sup> , Others <sup>a</sup>	-
VitalDB	ICU patients	6,090	ECG, PPG <sup>a</sup> , ABP <sup>a</sup> , Others <sup>a</sup>	Age, Gender, Height, Weight, BMI
University of Queensland Vital Signs Dataset	Anesthesia patients	32	ECG, PPG, ABP, CO2, EEG <sup>a</sup> , Others <sup>a</sup>	-

Figure 10: List of datasets used for training DNN ABP Estimation models [43]

For a continuous ABP waveform output, slight alterations in the PPG input features from the training data features may lead to a shift in input space. If the shift in input space is significant enough, the ABP waveform prediction model may become invalid causing an inaccurate output. For example, older age affects PPG pulse wave features, which can be seen in Figure 11 [35].

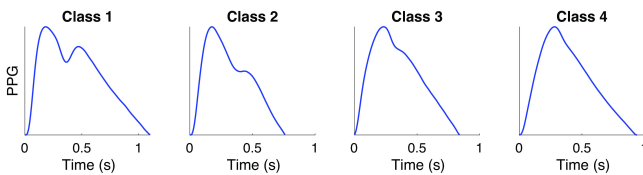


Figure 11: Multiple classes of PPG signals relative to age ranging from Class 1 (25) to Class 4 (65) [35]

### 2.5.2 MIMIC III

MIMIC III biosignals database comprises 67,830 record sets for approximately 30,000 ICU patients, with a median age of 65.8 years old. The record sets include time-synchronized PPG, ECG, & Invasive ABP waveforms [44].

The data acquisition setup for this database can be seen in Figure 12

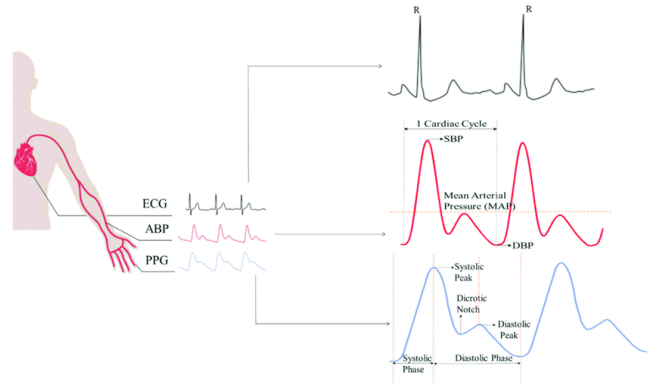


Figure 12: MIMIC III Data Acquisition Setup [41]

This database exclusively contains data from ICU patients, hence the signals are acquired using high-end medical equipment that is well-calibrated and monitored. ICU patients are immobile for long periods of time, which substantially increases the quality of the acquired data due to the lack of MA.

## 2.6 Gap in Literatures

Training the models with diverse datasets is necessary to achieve good performance in real-world applications. The problem lies in the lack of public ABP data in uncontrolled environments. Given the aforementioned, there is an evident gap in the literature for publications that explore the utility of ABP estimation models using single-sight PPG signals in uncontrolled/ semi-controlled settings. This gap is to be expected as the avenue of using DNN for Biosignal interpolation is still novel and is gaining interest momentum along the simultaneous rise of interest in Deep Learning as a whole sub-field.

There are additional limitations that affect the mass of literature that explores DNN ABP waveform estimation models using PPG only. Most publications train DNN with PPG & ECG. The multi-modality adds robustness to the system as it provides more information to the model from which a more accurate prediction model can be constructed. Multi-modal features are also harder to corrupt with noise that affects only one of the multi-modalities. Therefore, more publications use ECG + PPG inputs to DNN models that estimate ABP waveform. The MIMIC III public database also contains ECG signals. The limitation imposed by the lack of data availability makes the PPG + ECG option more favorable.

To explore further, this report will analyze the effect of a few basic daily activities on PPG data and then examine the influence of the PPG data on the ABP waveform output of DNN model. Utilizing wrist PPG is specifically desirable since it broadens the PPG data availability the most since its widespread integration

with smartwatches. Up to date, no other publication attempted diversifying the data setting and condition on continuous ABP estimation using wrist PPG

### 3 Methodology

#### 3.1 System Overview

In this assignment, a DNN developed & trained by Ibtehaz et al. [45], will be set up and tested with PPG data collected from a wearable watch. The data will be processed to match the properties of the MIMIC III data. Following, the PPG segments’ quality will be assessed and classified as either good or bad quality. For Further assessment of input, the time and frequency plots of segments will be qualitatively inspected and compared to optimal references of their subsequent plots.

Good quality signals will be used as input to the model, and the corresponding ABP output segment will be examined qualitatively in comparison to the input and to the ideal waveform feature from Figure 3. The whole system in this report is coded in Python. The computer running the system uses an AMD Ryzen 7 6800HS.

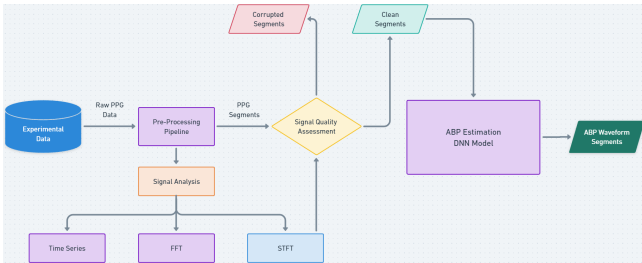


Figure 13: System Overview

#### 3.2 Experimental Design

##### 3.2.1 Ethical Approval

The following protocol received approval for this protocol from the Computer Information Sciences (CIS) Ethics Committee at the University of Twente. The committee reviewed the ethical aspects of this project and concluded that it raised no ethical concerns.

##### 3.2.2 Protocol

An experimental protocol is designed to collect wrist PPG signals from 2 healthy participants with no history of CVD. The PPG data will be used for testing the model that estimates the ABP waveform.

The identity of the participants will remain anonymous, and will not be shared with any third party. None of the

participants had an allergy to rubber, the material from which the wristband is made.

Prior to the beginning of the protocol, an initial BP measurement was taken; this will be used for denormalization of output as  $SBP_{ref}$  &  $DBP_{ref}$  in Eq 3 & 4, respectively.

The List of activities can be seen in Table 3

Activity	Duration [min]	Intensity
[A1] Static (sit)	2	.
[A2] Finger Tapping (sit)	2	Low
[A3] Standing	2	.
[A4] Walking	2	$\approx 0.8 \frac{m}{s}$

Table 3: Experimental Protocol Activities

Since PPG is an optical method, the two participants were chosen to have different skin tones and arm hair density, to test the effects of these variables on the results. Skin tone was categorized based on the Fitzpatrick scale, seen in Figure 14, and hair density was assessed qualitatively using the scale in Figure 15 [46]. Wrist circumference was also measured.

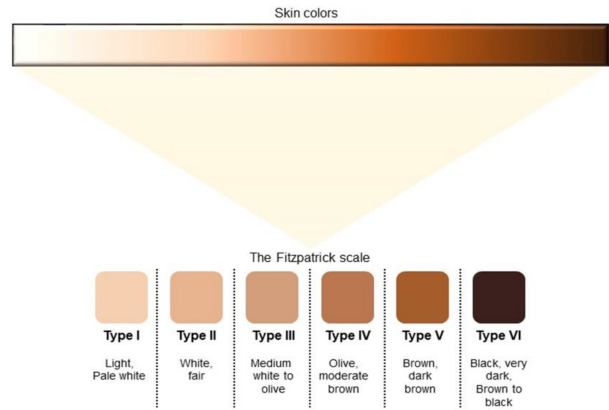


Figure 14: Fitzpatrick Scale [46]

Both participants consented to share the information in Table 4. This information was taken for the sake of completeness in case any of these variables affected the data acquisition.

Variable	P1	P2
Age	22	22
Skin Tone	Type I	Type IV
Hair Density	Sparse	Dense
Wrist Circumference [cm]	16.2	15.7

Table 4: Participants Information



Figure 15: Photographic Forearm Hair Scale [47]

### 3.2.3 Equipment

The wristwatch that was used to collect PPG signals is Empatica’s E4 [48].

E4 is a research-grade wristwatch equipped with multiple bio-sensors, including PPG, to provide real-time biometric data. Several studies have used E4 for several purposes, most popularly to examine HR variability under resting conditions [49] [50].

The device streamed the real-time PPG data from each recording via Bluetooth to a smartphone then the data was transferred to the personal computer that will run the model. The specifications of the device can be seen in table 5

<b>Manufacturer</b>	Empatica E4
	Empatica Inc, Boston, MA, US
<b>Certification</b>	CE class IIa
<b>Body position</b>	Wrist, ankle
<b>Biosignals</b>	ACC, EDA, PPG, TEMP
<b>Sampling rates</b>	32 Hz, 4 Hz, 64 Hz, 4 Hz
<b>ACC range</b>	$\pm 2$ g
<b>Battery life</b>	24-48 h
<b>Recording mode</b>	Device, streaming

Table 5: Specifications of Empatica E4 [51]

As per Empatica’s instructions, the E4 was fitted on the user in the manner shown in Figure 16.

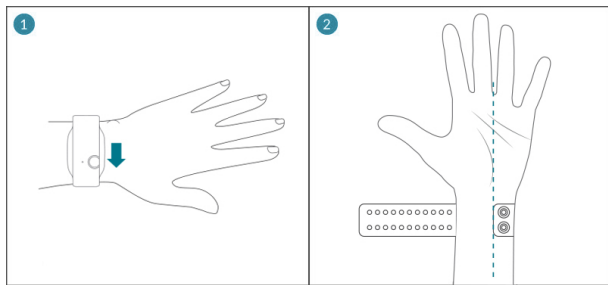


Figure 16: E4 correct positioning on the wrist [52]

The reference measurements were taken with a digital sphygmomanometer, similar to the one in Figure 1.

## 3.3 Neural Network Model

The implemented estimation is comprised of two-stage cascading U-NET, the first for approximating the ABP waveform, and the second is for refining the output waveform. The data pipeline can be seen in Figure 17

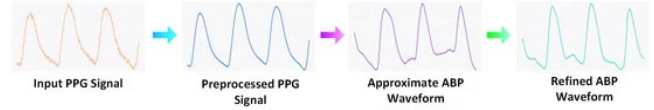


Figure 17: Data Pipeline Overview [45]

U-NET is a symmetrical encoder-decoder neural network architecture. It is conventionally used for biomedical image semantic segmentation. This model is a 1D variant instead of the more commonly used 2D U-NET. A few papers used this architecture for continuous ABP estimation with high prediction accuracy [53] [45].

The model was trained with a subset of the MIMIC III database. 10-Fold Cross-Validation was used by iterative training with 90% of the data and testing with the other 10% to find the better-performing model parameters.

The model achieved a prediction mean absolute error (MAE) for DBP of  $3.449 \pm 6.147$  mmHg, SBP of  $2.310 \pm 4.437$  mmHg, and Mean Arterial pressure (MAP) of  $5.727 \pm 9.162$  mmHg.

These results pass the British Hypertension Society’s (BHS) Grade A standard and the criterion set by the Association for the Advancement of Medical Instrumentation (AAMI) for BP measurement instrumentation [54].

The specific architecture of the model is not a bottleneck for ABP prediction as several models have already achieved similar performance. Hence, this method was chosen as it provides excellent prediction performance with clean input while being thoroughly documented by Ibtihaz et al [45].

An overview diagram of the model’s architecture can be seen in Figure 18.

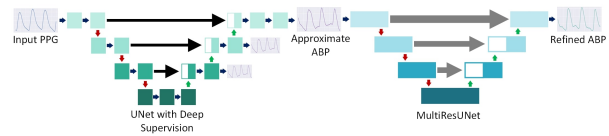


Figure 18: [45]

## 3.4 Preprocessing

### 3.4.1 Sample Rate Conversion

The input PPG data was upsampled from 64 to 125 Hz. The method chosen to upsample the input data is cubic

spline interpolation upsampling. This method was chosen as it provides high smoothness and accuracy, both of which are necessary to maintain the features of biosignals like PPG.

Cubic spline interpolation works by fitting third-order polynomials between each two sample points of the input and then resampling the signal at the desired rate.

### 3.4.2 Bandpass Filter: ChebyshevII

PPG signals contain undesired components such as low-frequency baseline wander caused by respiration rate & changes in blood perfusion [55] [20]. All the pertinent frequency harmonics of PPG pulse wave line in between 0.5 to 8 Hz [56].

For this assignment, only the pulsatile component of the PPG signal is needed, hence a bandpass filter was implemented to filter out these undesired components. A 5th-order ChebyshevII bandpass filter was chosen specifically as it preserves pulse wave features more than other popular filters such as Butterworth filter [57] [58] [43]. The high-order filter has a steeper negative slope between the cutoff frequency and the stop band, which comes at the cost of being more computationally demanding than a lower-order filter.

The passband range is [0.5 8] Hz, as stated earlier, and the stopband ripple was set to 0.5 dB for minimal interference from filtered bands.

### 3.4.3 Segmentation & Normalization

$$X = \begin{bmatrix} x_1 \\ x_2 \\ x_3 \\ \vdots \\ x_N \end{bmatrix} \quad (1)$$

The input of the DNN is the 1024 samples of each 8.192-second segment, sampled at 125 Hz. The E4’s PPG data was segmented as such followed by the normalization of the amplitude of each signal segment to range between [0 1]. The normalization was done to each segment data vector  $\vec{X}$  by substituting it into equation 2;  $X_{min}$  &  $X_{max}$  is the minimum and maximum input values of .

$$\vec{X}_{norm} = \frac{\vec{X} - X_{min}}{X_{max} - X_{min}} \quad (2)$$

Since the proposed DNN was trained and tested with ground truth ABP data, it only outputs normalized ABP segments. To denormalize the output amplitude, reference measurements were taken from the participants as stated earlier, and used instead of the missing maximum

( $ABP_{max}$ ) and minimum ( $ABP_{min}$ ) values in equations 3 & 4, respectively.

BP can fluctuate by 5% intermittently under resting conditions, so the reference values are adjusted with this margin accordingly [59].

This adds uncertainty to the precision of the output in terms of baseline and scaling. However, this does not affect the features of the output signal which will be the main focus of the results.

$$ABP_{max} = SBP_{ref} * 1.05 \quad (3)$$

$$ABP_{min} = DBP_{ref} * 0.95 \quad (4)$$

### 3.4.4 Signal Quality Assessment

Qualitatively, PPG pulses can be classified into 3 categories: Excellent (G1), Acceptable (G2), and Unfit (G3) for diagnostic purposes. G1 is described as having clear [60] Most of the training data of the proposed DNN are of the G1 & G2 category, as all the G3 segments were removed from the dataset that trained and tested the model.

Therefore, E4’s data segments need to be assessed in terms of signal quality for the model to correctly predict the output waveform as the model was not trained to compute prediction with noisy inputs.

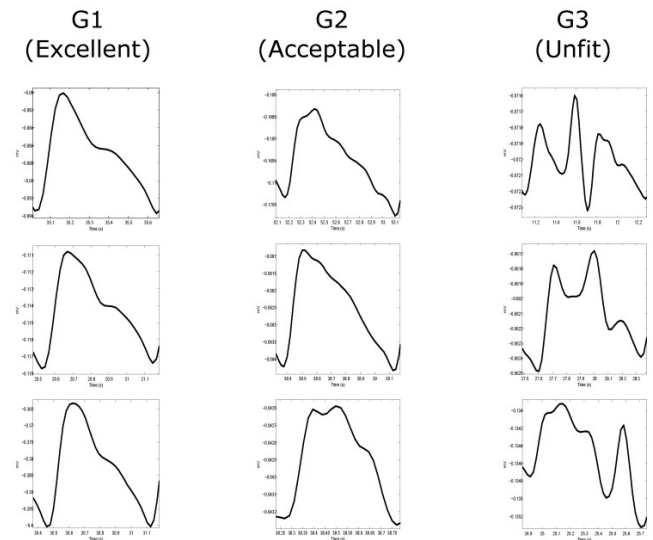


Figure 19: Categories of PPG Pulse Wave Quality [60]

To observe the data composition of each segment more objectively, the discrete short-time fourier transform (STFT) of each segment was computed and plotted on a spectrogram. STFT gives a better perspective on the pulsatile nature of each segment as it combines both time and frequency information, although to a lesser resolution than both [61].

With each peak, the signal energy spikes. The temporal locality of each peak can be used to count beats per segment, and the energy of each peak is concentrated within a certain frequency band.

These properties were used to identify and discard low-quality. The total energy of the highest intensity STFT time sample is taken and used as a reference for the rest of the pulses.

$$\mathbf{S}_{FT} = \begin{bmatrix} S_{11} & S_{12} & \cdot & \cdot \\ S_{21} & S_{22} & \cdot & \cdot \\ \cdot & \cdot & \cdot & \cdot \\ \cdot & \cdot & \cdot & \cdot \end{bmatrix} \quad (5)$$

From matrix 5, if each column defined  $\vec{s}$ , the column with the highest energy result when used in equation 6 is  $\vec{s}_{ref}$ .

$$E_s = \sum_{i=0}^{N-1} |s[i]|^2 \quad (6)$$

By iteratively taking the difference between the energy of  $\vec{s}_{ref}$  and the energy of each  $\vec{s}$  in  $\mathbf{S}$ , a threshold energy ratio can be set to detect data discrepancies over time.

$$E_{ratio} = \frac{|E_s|}{|E_{ref}|} \quad (7)$$

For each instant where the ratio exceeds that threshold, a beat is counted with variable  $r$  starting from zero.

$$\mathbf{IF}(E_{Thresh} < E_{ratio}) : r = r + 1 \quad (8)$$

Given that a healthy person’s resting HR lies in the range of [60 90] BPM, a good quality segment will have the threshold exceeded 7 to 11 times by the end of the segment, no more & no less.

$$7 \leq r \leq 13 \quad (9)$$

This way, if the segment contains an inconsistent pulse(s) or a relatively high spike, then the  $\vec{s}_{ref}$  will be the anomaly vector and the whole segment will be discarded. The threshold value through trial and error to eliminate the corrupted G3 signals while passing G2 and G1 signals as much as possible, based on the 3 categories in Figure 19.

The discrete wavelet transform (DWT) was considered but was not chosen as it is more computationally demanding than STFT without necessarily offering better time-frequency resolution.

The Fast Fourier Transform (FFT) of the whole segment will also be computed and plotted to gain insight into the prominent frequency components of both high and low-quality signals. FFT offers a broader image of the signal composition than STFT, but given that a clean segment has clean harmonics, a corrupted signal can be easily identified.

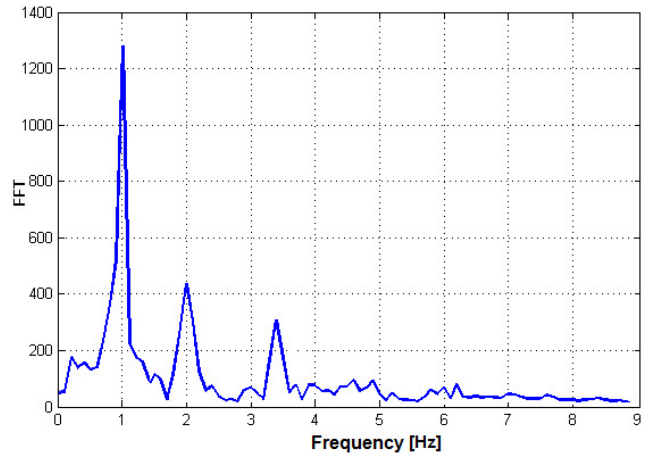


Figure 20: Ideal FFT for PPG Segment [31]

Skewness also highly correlates with PPG signal quality [60]. Skewness is a statistical measure of the asymmetry of the sample distribution around the mean. Skewness is calculated using equation 10. Skewness will be used to assess signal quality however it will not be used to eliminate signals based on its result.

$$\text{Skew}[X] = \frac{1}{N} \sum_{i=1}^N \left( \frac{x_i - \mu}{\sigma} \right)^3 \quad (10)$$

In equation 10,  $\mu$  refers to the mean, and  $\sigma$  refers to the standard deviation of each segment.

## 4 Results

### 4.1 Model Setup

To start, The model was set up and tested with a segment of the MIMIC III data to verify that the model was working properly prior to testing with the experimental data. The data processing pipeline, seen in Figure 17 from raw PPG data to ABP output takes anywhere from 0.8 to 3 seconds per 1024 sample-long segment. The resulting output can be seen in Fig 21

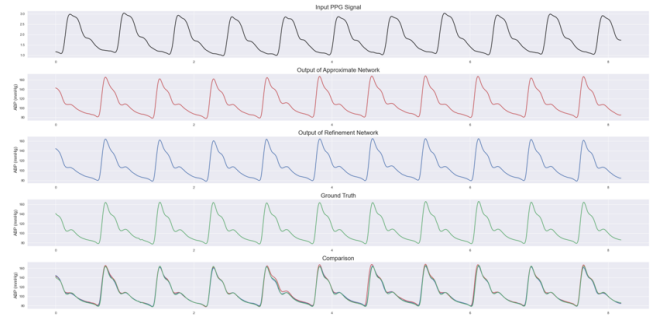


Figure 21: Model output for random MIMIC III Segment

## 4.2 Pre-Processing

The preprocessing stages all worked successfully. In Figure 22, the raw and upsampled pulse wave can be seen to completely overlapping

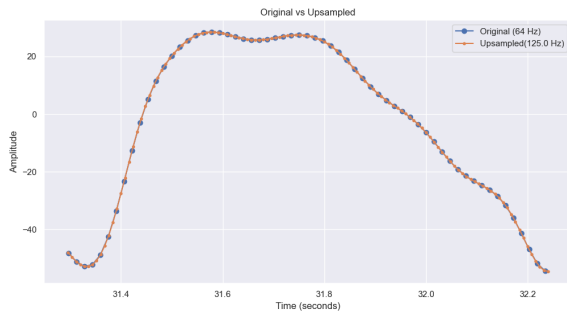


Figure 22: 64 to 125 Hz Upsampled

As can be seen in Figure 23 The Chebyshev II filter flattened the pulse waves slightly but maintained their overall shape. Small variations in amplitude should not cause the prediction model as most of the morphological features were maintained.

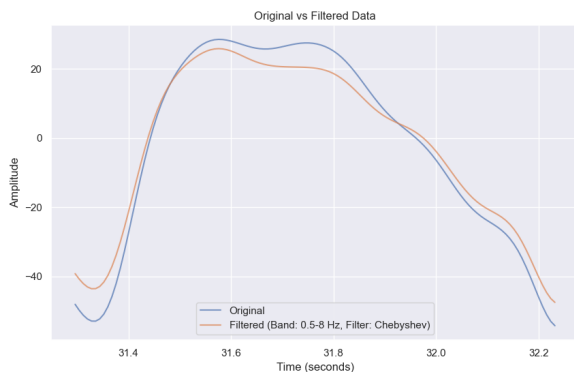


Figure 23: Bandpass Filter vs Unfiltered Pulse Wave

## 4.3 Experimental Data Analysis

### 4.3.1 Static [A1 & A3]

Given that no motion occurred, signals acquired from both participants, while standing and sitting, exhibited the expected morphological features of a clean PPG pulse wave, relative to Figure 4.

It can be seen from Figures 24 & 25, that the waveform is class A relative to the categorization in Figure 11. This is to be expected given both participants were under 25.

The Skewness of clean segments, from both participants, ranges between -0.6 to -0.3.

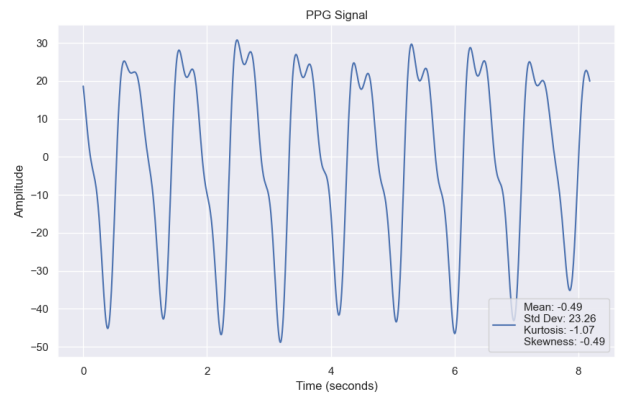


Figure 24: Example of clean A1 segment

While standing up, systolic peaks have a higher amplitude and a more pronounced notch. This was the case for both participants as well.

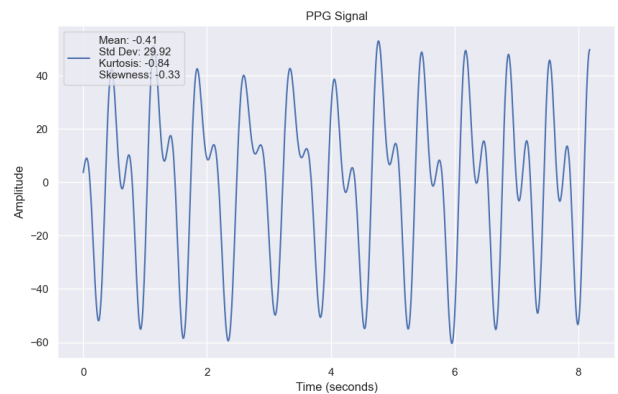


Figure 25: Example of clean A3 segment

As can be seen in Figure 26, the FFTs of clean segments are nearly identical to the reference FFT in Figure 20.

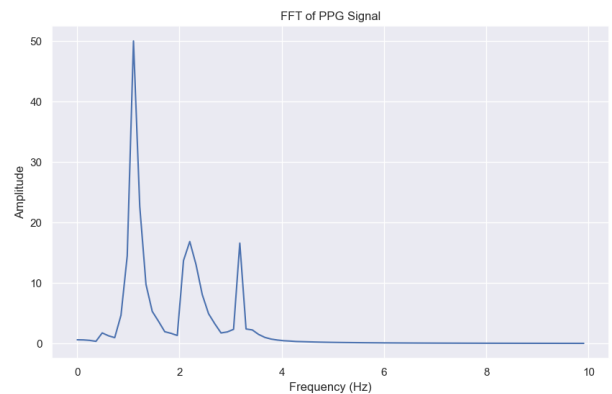


Figure 26: FFT: Fig 25

In Figure 27, each systolic peak appears as an intense

line, and all the lines are composed of similar frequency content with similar intensity.

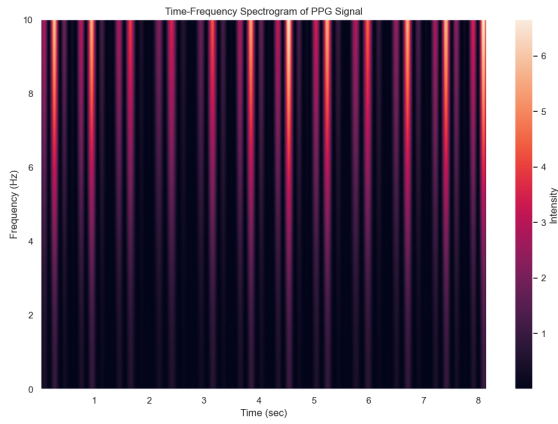


Figure 27: Spectrogram: Fig 25

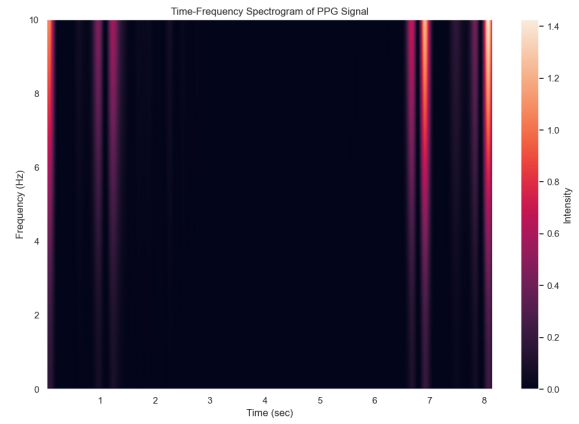


Figure 29: Spectrogram: Fig 28

While walking, the noise is significantly more powerful. This can be seen in Figure 30

### 4.3.2 Dynamic [A2 & A4]

None of the data segments acquired from finger-tapping and walking was classified as high quality. In Figure 28, an example of a noisy PPG segment, taken from finger-tapping, data can be seen.

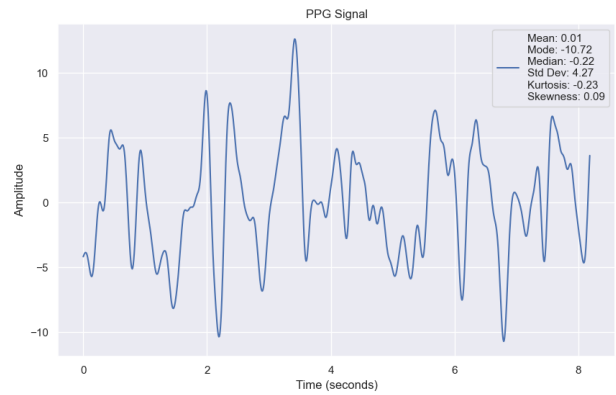


Figure 30: Example of A4 Segment

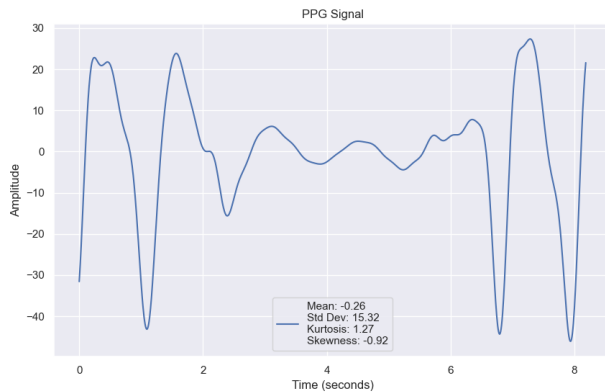


Figure 28: Example of Noisy A2 Segment

It can be inferred from the FFT in Figure 31, that the noise bandwidth overlaps with the 3 PPG frequency components.

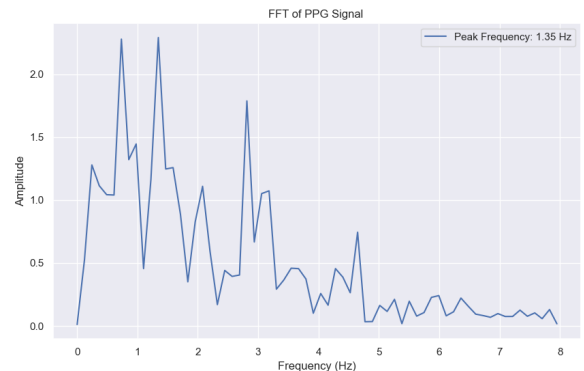


Figure 31: FFT: Fig 30

From the spectrogram in Figure 29, the visible lack of pulses indicates the low quality of segment 28

### 4.3.3 SQA

The threshold parameter was tuned iteratively to find its optimal value. With each iteration, the classified segments were observed, and based on the accuracy of the assessment the threshold was adjusted. The optimal threshold was 0.53 for P1 and 0.47 for P2.

During static conditions, 64.55 % of PPG segments passed the SQA for P1 and 56.16 % for P2.

All the segments acquired during dynamic activities were rejected due to the abundance of MA.

The assessment outcome of all segments from each activity per participants each participant can be seen in table 6

Activity	P1		P2	
	✓	×	✓	×
A1	28	10	22	14
A2	0	38	0	35
A3	23	18	19	18
A4	0	37	0	39

Table 6: Good vs Bad Quality PPG Segments Per Activity Per Participant

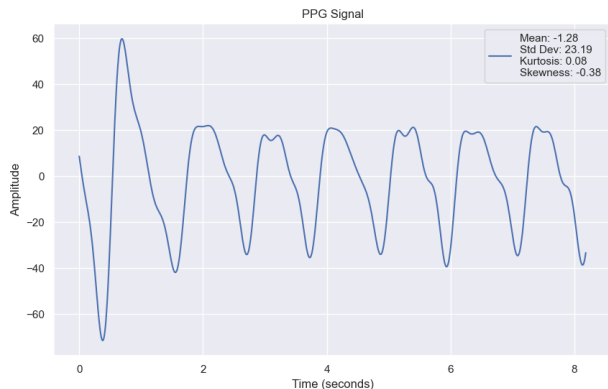


Figure 32: Example of Rejected Segment

### 4.4 ABP Output

The model outputs clean ABP waveforms, given that the corresponding input segment is clean as well. The MAP of all the segments that passed the SQA is 89.92 mmHg for P1 and 94.01 mmHg for P2. The accuracy of this value can not be qualitatively assessed.

In Figures 33 & 34, the morphological features of the output waveforms are in line with what is to be expected; most pulse waves have a clear peak and notch.

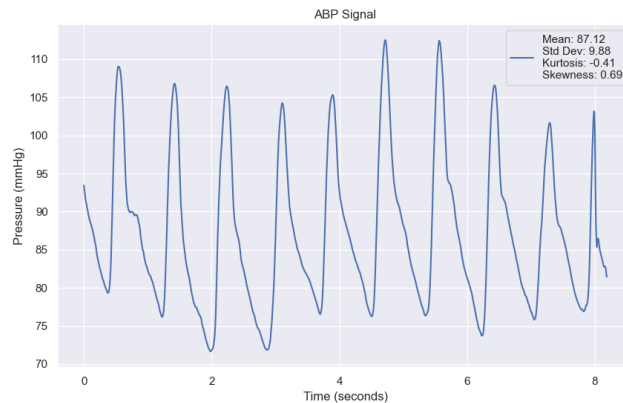


Figure 33: ABP Waveform Output (P1)

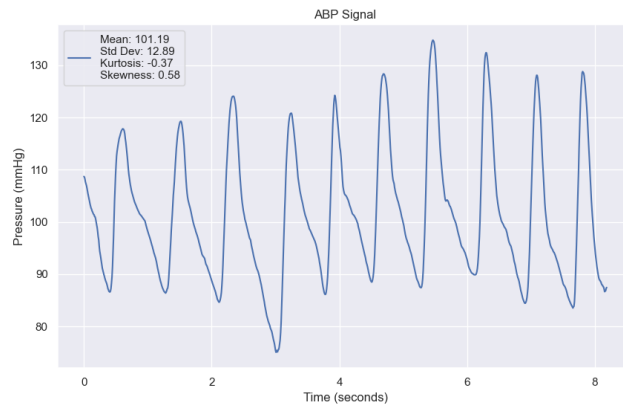


Figure 34: ABP Waveform Output (P2)

Strong oscillatory behavior in the PPG pulse wave distorted the output pulse wave. The distortion scaled with the oscillation component between the peak and notch. This can be attributed to the young age of the participants as seen in Figure 11.

The distortion can be seen in Figure 35

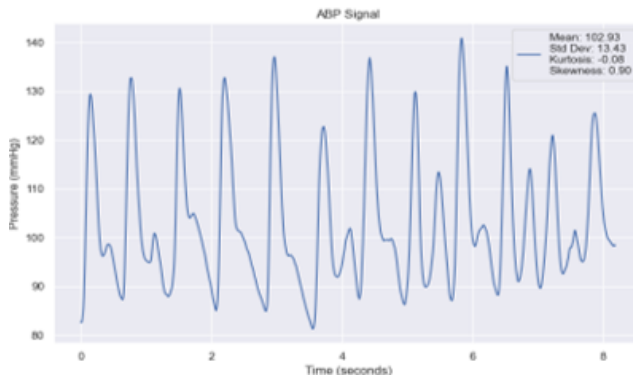


Figure 35: ABP Output of PPG Segment in Figure 25

In figure 36, the output waveform of a noisy input can

be seen. No clear distinction between pulses can be made, and all the pulse wave features are unrecognizable.

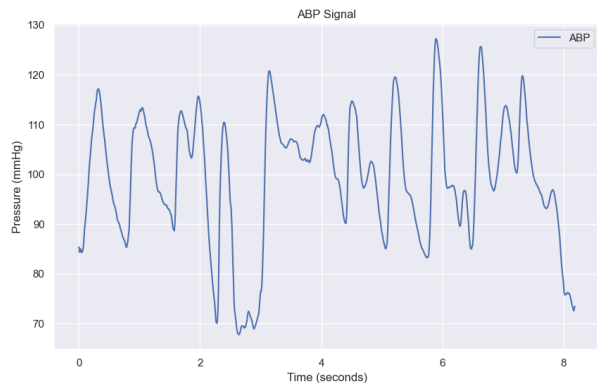


Figure 36: ABP Estimate for Rejected PPG Segment in Figure 30

## 5 Discussion

### 5.1 E4 & PPG Signal Quality

The E4’s PPG sensor has proven to be very susceptible to MA.

The rejected segment, seen in Figure 32, was taken during a static measurement. The participant had a tremor which caused the oscillatory interference at the start of the segment. While reviewing the E4 integrated accelerometer data, several instances of slight tremors were seen as an intermittent deviation in position. An example of this is in Figure 37.

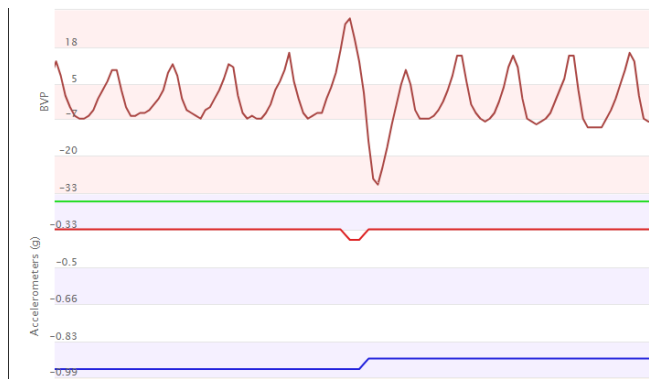


Figure 37: Example of Motion Artifacts  
Top: Raw PPG  
Green, Red, Blue: ACC Z, X, Y

Active MA reduction is a must for any application that requires PPG feature extraction. Accelerometer data has been used in MA reduction techniques for PPG signals [24]. Since the E4 is equipped with a 3-axis accelerometer, it can be capitalized for MA reduction with no external sensors. In some segments, slight MA were present but

the E4’s accelerometer did not pick up the motion. For the aforementioned, the proposed system setup is not fit for ABP estimation during dynamic activities.

In a publication by Böttcher et al., the E4’s PPG data quality was examined throughout the day from six in and outpatient cohorts. The study found that during the night the PPG data segments were up to 40 % higher quality than during the daytime primarily due to the lack of MA [51]. A heatmap representation of E4’s PPG quality can be seen in Figure 38.

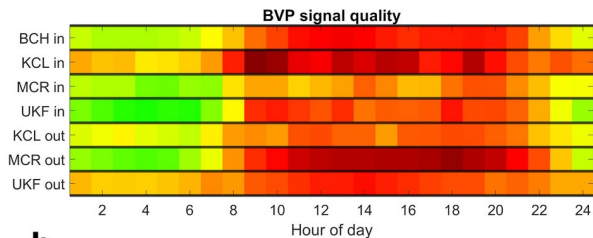


Figure 38: 24H Heatmap of E4’s PPG quality [51]  
Red: Lower Quality - Green: Higher Quality

The better night-time data quality makes the proposed system much more effective for sleep monitoring. The ABP estimation model can provide key insights into the hemodynamic changes induced by sleep apnea [62] [63].

### 5.2 Segment Quality Assessment

The Bandpass filter eliminated the baseline wander caused by the respiratory rate. However, baseline wander is one of three respiratory modulations, the other two being amplitude and frequency modulation [64].

Some segments with high amplitude modulation were classified as low-quality and discarded despite all the segments’ pulse waves being morphologically accurate. The increased amplitude of the systolic peaks over the segment period caused the assessment algorithm to take the peak pulse’s energy as a reference. The energy of the reference peak was significantly higher than the rest of the peaks which excluded the count of clean pulse waves as the ration was below the set threshold. An example of an amplitude-modulated segment can be seen in Figure 39.

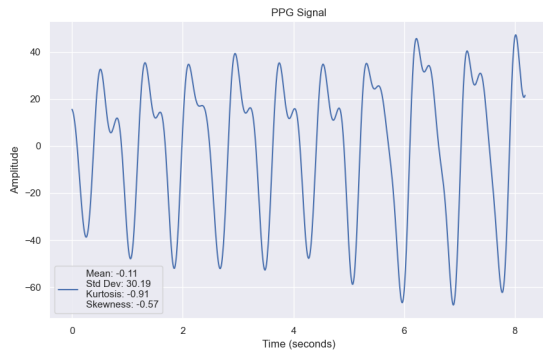


Figure 39: Amplitude Modulated PPG Segment

The modulation effects do not pose a problem as the training data was also not de-modulated. So the model could use the modulation properties as features in the estimation process.

The SQA algorithm proposed in this report can be used as a preliminary filter that passes the most consistent segments only. A second SQA algorithm could follow that examines the segments deemed corrupted by the first one. The second SQA could compute the cross-correlation between periodic peaks in the segment to establish consistency between each peak and the rest. A segment of similar behavior to the one in Figure 32 is salvageable using an MA reduction technique as the noise component is both intermittent and does not dominate the pulse amplitude.

Skewness was a poor metric of signal quality for the acquired data in this assignment as several low-quality segments had similar skewness to high-quality signals. This was also observed by Ibtehaz et al. [45].

### 5.3 System Design

The U-NET model used in this assignment has two key problems.

The first problem is the normalized output waveform as denormalizing it requires maximum and minimum ABP values. Hence, using it with no ground truth data adds to the output error in terms of scale and offset. To counteract this problem, another prediction model can be added before the U-NET’s input to estimate the SBP & DBP values for the denormalization of the waveform output.

The added system will likely be another regression model that suffers from the same problem that U-NET has, lack of diverse training data. The errors of both systems will aggregate. And while this solution could work, the computational complexity of the whole system will increase drastically relative to the value of gained information.

The second problem is the input segment length being too long. As shown earlier, intermittent interference can cause a segment to be discarded as low quality despite the segment containing multiple clean pulse waves as in Figure 32. This wastes usable data that can produce more accurate estimations over time. With shorter input segment length and the implementation of an MA reduction method, the number of high-quality output segments can increase substantially.

U-NET only uses the samples of the PPG segment as input and implicitly does the feature extraction within the network. An improved model would also intake other data such as the age and height of participants. Personal biometrics allow DNN models to create better predictions of ABP by accounting for changes in input features caused by these biometrics. Hence, the model would have a different abstraction of the output as the participants’ age differs to mitigate the effect seen in Figure 35.

## 6 Conclusions

In this assignment, The utility of PPG signals to estimate is explored and tested. Salient methods for ABP measurement were analyzed and evaluated for their pros and cons. Utilizing DNN was found to be the common theme in this area of research as the advent of advanced deep learning architectures bolstered researchers’ ability to extrapolate ABP waveforms from biosignals such as PPG signals only.

The core drawback of relying solely on DNN prediction capabilities is the lack of ABP ground truth data as only one publicly available database contains time-synchronized ABP waveform and PPG. The estimation accuracy presented as “state-of-the-art” by many publications was only achieved on testing data from the same database (MIMIC III). Furthermore, acquiring ABP and PPG data poses a difficult hurdle as continuous ABP waveforms are measured invasively. This constricts the data acquisition to exclusively controlled environments and the demographic from which data is acquired to critical patients only. These issues led to a shortage of ABP data collected during dynamic activities in uncontrolled environments from diverse populations in terms of Age, Cardiovascular Health, etc.

The MIMIC III biosignals database contains clean data only as critical ICU patients are less likely to be mobile so motion artifacts are circumvented. Unlike widespread PPG sensors in daily smartwatches, ICU PPG sensors are medical grade and optimized for the highest quality data acquired. This leads to a disparity in quality between the MIMIC III data and data acquired using daily wearables. And since DNN models are trained on ICU PPG data, data from daily wearables may not be adequate for the ABP estimation performed by DNN in terms of quality,

SNR, precision, and sampling rate.

To examine the issue further, a model was adopted from another publication [45] that designed and trained a 2-stage cascading DNN to perform 1-to-1 regression from 8.192 second PPG signal segments to 8.192 ABP signal segments. The model passed the BHS and the AAMI standards criteria for accurate BP measurements.

PPG data from both static and dynamic activities was acquired using a wristwatch with embedded PPG and accelerometer sensors to gain insight into the effects of activities on PPG signals.

A preprocessing pipeline was composed and coded to process the data properties and clean the signal components from undesired influences.

The STFT, FFT, and several statistical parameters were computed and plotted to evaluate the acquired signal quality in comparison to the optimal reference. A signal quality assessment algorithm was implemented using the STFT data to prune out corrupted signals prior to the input of the ABP estimation model. The SQA was successful in its task however multiple segments were classified as corrupted due to minor fluctuations in pulse wave amplitude induced by MA and Amplitude modulation caused by respiratory.

The model successfully predicted a morphologically correct ABP waveform for up to 64.55 % of PPG segments acquired during static conditions. However, the model failed to estimate any coherent outputs from dynamic activities as these input segments were corrupted with motion artifacts. Certain effects on PPG signals that are affected by age caused the model to distort the output signal which discounts it for reliable use in younger individuals.

The high susceptibility of PPG to MA makes the proposed system a poor fit for ABP estimation during daily activities. The ABP waveform estimates can not be validated due to the lack of ground truth ABP data. Nonetheless, with an added MA reduction technique and a more capable SQA algorithm, the system shows promise in monitoring ABP under static semi-controlled conditions in older individuals.

## 7 Acknowledgements

This report demonstrates the work aggregate of the B.Sc. Engineering thesis of Moustafa Mahmoud under the supervision of Dr. Ying Wang, Dr. Kuan-Hsun Chen, and M.Sc. Yaowen Zhang; Members of the Department of Biomedical Signals and Systems (BSS) at The University of Twente.

## References

- [1] “Global status report on noncommunicable diseases 2014 ”attaining the nine global noncommunicable diseases targets; a shared responsibility”.
- [2] “Checkups and tests you shouldn’t miss.” <https://www.webmd.com/a-to-z-guides/ss/slideshow-checkups-needed>, 2022. [Online; Accessed: Oct 8, 2023].
- [3] K. T. Mills, A. Stefanescu, and J. He, “The global epidemiology of hypertension,” 4 2020.
- [4] A. V. Chobanian, G. L. Bakris, H. R. Black, W. C.ushman, L. A. Green, J. L. Izzo, *et al.*, “The seventh report of the joint national committee on prevention, detection, evaluation, and treatment of high blood pressure: the jnc 7 report,” *JAMA*, vol. 289, no. 19, pp. 2560–2572, 2003.
- [5] “Understanding blood pressure readings.” <https://www.heart.org/en/health-topics/high-blood-pressure/understanding-blood-pressure-readings>, 2023. [Online; Accessed: Oct 19, 2023].
- [6] G. Ogedegbe and T. Pickering, “Principles and techniques of blood pressure measurement,” 11 2010.
- [7] B. Lee, J. H. Jeong, J. Hong, and Y. H. Park, “Correlation analysis of human upper arm parameters to oscillometric signal in automatic blood pressure measurement,” *Scientific Reports*, vol. 12, 12 2022.
- [8] C. T. Goodman and G. B. Kitchen, “Measuring arterial blood pressure.”
- [9] G. Nuttall, J. Burckhardt, A. Hadley, S. Kane, D. Kor, M. S. Marienau, D. R. Schroeder, K. Handlogten, G. Wilson, and W. C. Oliver, “Surgical and Patient Risk Factors for Severe Arterial Line Complications in Adults,” *Anesthesiology*, vol. 124, pp. 590–597, 03 2016.
- [10] S. A. Esper and M. R. Pinsky, “Arterial waveform analysis,” 2014.
- [11] A. Yartsev, “Normal arterial line waveforms.” *Deranged Physiology*, Dec 2023. Available online: <https://derangedphysiology.com/main/cicm-primary-exam/required-reading/cardiovascular-system/Chapter%20760/normal-arterial-line-waveforms>.
- [12] Y. Nguyen and V. Bora, “Arterial pressure monitoring.” *StatPearls [Internet]*, Jan 2023.
- [13] A. Ghaffari, M. R. Homaeinezhad, M. Akraminia, and M. Davaeaha, “Finding events of electrocardiogram and arterial blood pressure signals via discrete wavelet transform with modified scales,” *Proceedings*

of the Institution of Mechanical Engineers, Part H: Journal of Engineering in Medicine, vol. 224, pp. 27–42, 1 2010.

- [14] J. Allen, “Photoplethysmography and its application in clinical physiological measurement,” *Physiological measurement*, vol. 28, no. 3, p. R1, 2007.
- [15] M. M. P., N. V., and V. J.C., “Spot and continuous monitoring of heart rate by combining time and frequency domain analysis of photoplethysmographic signals at rest conditions,” *IET Signal Processing*, vol. 11, no. 9, pp. 1076–1082, 2017.
- [16] A. Pantelopoulos and N. G. Bourbakis, “A survey on wearable sensor-based systems for health monitoring and prognosis,” *IEEE Transactions on Systems, Man, and Cybernetics, Part C (Applications and Reviews)*, vol. 40, no. 1, pp. 1–12, 2010.
- [17] ResearchAndMarkets.com, “Global ppg biosensors market report 2021-2028: Increasing demand for smart wearables incorporated with ppg biosensors,” *Business Wire*, 2021.
- [18] B. Roy and R. Gupta, “Modtrap: Improved heart rate tracking and preprocessing of motion-corrupted photoplethysmographic data for personalized healthcare,” *Biomedical Signal Processing and Control*, vol. 56, 2 2020.
- [19] P. H. Charlton, K. Kotzen, E. Mejía-Mejía, P. J. Aston, K. Budidha, J. Mant, C. Pettit, J. A. Behar, and P. A. Kyriacou, “Detecting beats in the photoplethysmogram: Benchmarking open-source algorithms,” *Physiological Measurement*, vol. 43, 8 2022.
- [20] P. H. Charlton, J. Allen, R. Bailon, S. Baker, J. A. Behar, F. Chen, G. D. Clifford, D. A. Clifton, H. J. Davies, C. Ding, X. Ding, J. Dunn, M. Elgendi, M. Ferdoushi, D. Franklin, E. Gil, M. F. Hassan, J. Hernesniemi, X. Hu, N. Ji, Y. Khan, S. Kontaxis, I. Korhonen, P. A. Kyriacou, P. Laguna, J. Lazaro, C. Lee, J. Levy, Y. Li, C. Liu, J. Liu, L. Lu, D. P. Mandic, V. Marozas, E. Mejía-Mejía, R. Mukkamala, M. Nitzan, T. Pereira, C. C. Y. Poon, J. C. Ramella-Roman, H. Saarinen, M. M. H. Shandhi, H. Shin, G. Stansby, T. Tamura, A. Vehkaoja, W. K. Wang, Y.-T. Zhang, N. Zhao, D. Zheng, and T. Zhu, “The 2023 wearable photoplethysmography roadmap,” *Physiological Measurement*, 7 2023.
- [21] P. Martín-Escudero, A. M. Cabanas, M. L. Dotor-Castilla, M. Galindo-Canales, F. Miguel-Tobal, C. Fernández-Pérez, M. Fuentes-Ferrer, and R. Giannetti, “Are activity wrist-worn devices accurate for determining heart rate during intense exercise?,” *Bioengineering*, vol. 10, 2 2023.
- [22] M. A. Almarshad, M. S. Islam, S. Al-Ahmadi, and A. S. BaHammam, “Diagnostic features and potential applications of ppg signal in healthcare: A systematic review,” *Healthcare (Basel)*, vol. 10, no. 3, p. 547, 2022.
- [23] J. Lee and K. Matsumura, “Motion artifact reduction in photoplethysmography using independent component analysis,” *IEEE Transactions on Biomedical Engineering*, vol. 65, no. 3, pp. 692–700, 2018.
- [24] D. Pollreisz and N. TaheriNejad, “Detection and removal of motion artifacts in ppg signals,” *Mobile Networks and Applications*, vol. 27, pp. 728–738, 4 2022.
- [25] D. Seok, S. Lee, M. Kim, J. Cho, and C. Kim, “Motion artifact removal techniques for wearable eeg and ppg sensor systems,” *Frontiers in Electronics*, vol. 2, 5 2021.
- [26] I. C. S. Society, D. da xue, C. A. of Automation. Technical Committee on Control, D. of Cyber Physical Systems, I. S. S. I. E. Chapter, C. da xue, I. of Electrical, and E. Engineers., *Proceedings of the 29th Chinese Control and Decision Conference (2017CCDC) : 28-30 May 2017, Chongqing, China*.
- [27] C. L. Chang and L. Wang, “Study on the tolerance of motion artifacts in estimating variance of blood pressure by single ppg,” vol. 2685, American Institute of Physics Inc., 5 2023.
- [28] B. Bent, B. A. Goldstein, W. A. Kibbe, and J. P. Dunn, “Investigating sources of inaccuracy in wearable optical heart rate sensors,” *npj Digital Medicine*, vol. 3, 12 2020.
- [29] D. Castaneda, A. Esparza, M. Ghamari, C. Soltanpur, and H. Nazeran, “A review on wearable photoplethysmography sensors and their potential future applications in health care,” *International Journal of Biosensors Bioelectronics*, vol. 4, no. 4, pp. 195–202, 2018.
- [30] Y. K. Lee, J. Jo, and H. S. Shin, “Development and evaluation of a wristwatch-type photoplethysmography array sensor module,” *IEEE Sensors Journal*, vol. 13, no. 5, pp. 1459–1463, 2013.
- [31] S. Béres and L. Hejjel, “The minimal sampling frequency of the photoplethysmogram for accurate pulse rate variability parameters in healthy volunteers,” *Biomedical Signal Processing and Control*, vol. 68, p. 102589, 2021.
- [32] T. Gerardo, S. Adriana, A. C. M., P. Silvana, A. J. Martinez, M. Matías, S. F. Suarez, and B. S. H., “Photoplethysmogram’s amplitude is well correlated with beat-by-beat changes in arterial blood pressure,” *Clinical Medical Reviews and Case Reports*, vol. 8, 2 2021.

- [33] D. U. Jeong and K. M. Lim, “Combined deep cnn–lstm network-based multitasking learning architecture for noninvasive continuous blood pressure estimation using difference in ecg-ppg features,” *Scientific Reports*, vol. 11, 12 2021.
- [34] E. Brophy, M. D. Vos, G. Boylan, and T. Ward, “Estimation of continuous blood pressure from ppg via a federated learning approach,” *Sensors*, vol. 21, 9 2021.
- [35] P. H. Charlton, B. Paliakaité, K. Pilt, M. Bachler, S. Zanelli, D. Kulin, J. Allen, M. Hallab, E. Bianchini, C. C. Mayer, *et al.*, “Assessing hemodynamics from the photoplethysmogram to gain insights into vascular age: a review from vascagenet,” *American Journal of Physiology-Heart and Circulatory Physiology*, vol. 322, no. 4, pp. H493–H522, 2022.
- [36] W. H. Lin, F. Chen, Y. Geng, N. Ji, P. Fang, and G. Li, “Towards accurate estimation of cuffless and continuous blood pressure using multi-order derivative and multivariate photoplethysmogram features,” *Biomedical Signal Processing and Control*, vol. 63, 1 2021.
- [37] Y. Cao, H. Chen, F. Li, and Y. Wang, “Crisp-bp: Continuous wrist ppg-based blood pressure measurement,” pp. 378–391, Association for Computing Machinery (ACM), 10 2021.
- [38] S. Kanoga, T. Hoshino, S. Kamei, T. Kobayashi, T. Ohmori, M. Uchiyama, and M. Tada, “Comparison of seven shallow and deep regressors in continuous blood pressure and heart rate estimation using single-channel photoplethysmograms under three evaluation cases,” *Biomedical Signal Processing and Control*, vol. 85, 8 2023.
- [39] Pankaj, A. Kumar, R. Komaragiri, and M. Kumar, “A novel cs-net architecture based on the unification of cnn, svm and super-resolution spectrogram to monitor and classify blood pressure using photoplethysmography,” *Computer Methods and Programs in Biomedicine*, vol. 240, 10 2023.
- [40] B. C. Casadei, A. Gumiero, G. Tantillo, L. D. Torre, and G. Olmo, “Systolic blood pressure estimation from ppg signal using ann,” *Electronics (Switzerland)*, vol. 11, 9 2022.
- [41] T. Athaya and S. Choi, “A review of noninvasive methodologies to estimate the blood pressure waveform,” *Sensors*, vol. 22, p. 3953, 05 2022.
- [42] R. Srivignesh, “A walk-through of regression analysis using artificial neural networks in tensorflow.” <https://www.analyticsvidhya.com/blog/2021/08/a-walk-through-of-regression-analysis-using-artificial-neural-networks-from-the-ecg-flow/>, 2023. Accessed: [Insert access date here].
- [43] W. Wang, P. Mohseni, K. L. Kilgore, and L. Najafzadeh, “Pulsedb: A large, cleaned dataset based on mimic-iii and vitaldb for benchmarking cuff-less blood pressure estimation methods,” *Frontiers in Digital Health*, vol. 4, 2 2023.
- [44] A. E. Johnson, T. J. Pollard, L. Shen, L. W. H. Lehman, M. Feng, M. Ghassemi, B. Moody, P. Szolovits, L. A. Celi, and R. G. Mark, “Mimic-iii, a freely accessible critical care database,” *Scientific Data*, vol. 3, 5 2016.
- [45] N. Ibtehaz, S. Mahmud, M. E. Chowdhury, A. Khandakar, M. S. Khan, M. A. Ayari, A. M. Tahir, and M. S. Rahman, “Ppg2abp: Translating photoplethysmogram (ppg) signals to arterial blood pressure (abp) waveforms,” *Bioengineering*, vol. 9, 11 2022.
- [46] S. Mosca and A. Morrone, “Human skin pigmentation: From a biological feature to a social determinant,” *Healthcare*, vol. 11, no. 14, 2023.
- [47] L. von Schuckmann, M. C. Hughes, A. Green, and J. van der Pols, “Forearm hair density and risk of keratinocyte cancers in australian adults,” *Archives of dermatological research*, vol. 308, 11 2016.
- [48] E. Temperature, “E4 wristband — real-time physiological signals — wearable ppg, eda, temperature, motion sensors.” Empatica, 2020. Accessed: Jan. 15, 2024.
- [49] H. Stuyck, L. Dalla Costa, A. Cleeremans, and E. Van den Bussche, “Validity of the empatica e4 wristband to estimate resting-state heart rate variability in a lab-based context,” *International Journal of Psychophysiology*, vol. 182, pp. 105–118, Dec 2022.
- [50] A. A. T. Schuurmans, P. de Loeff, K. S. Nijhof, C. Rosada, R. H. J. Scholte, A. Popma, and R. Otten, “Validity of the empatica e4 wristband to measure heart rate variability (hrv) parameters: a comparison to electrocardiography (ecg),” *Journal of Medical Systems*, vol. 44, p. 190, Sep 2020.
- [51] S. Böttcher, S. Vieluf, E. Bruno, B. Joseph, N. Epitashvili, A. Biondi, N. Zabler, M. Glasstetter, M. Dümpelmann, K. V. Laerhoven, M. Nasserri, B. H. Brinkman, M. P. Richardson, A. Schulze-Bonhage, and T. Loddenkemper, “Data quality evaluation in wearable monitoring,” *Scientific Reports*, vol. 12, 12 2022.
- [52] Empatica Support, “Wear your e4 wristband.” <https://support.empatica.com/hc/en-us/articles/206374015-Wear-your-E4-wristband->, 2015. Accessed: Jan. 05, 2024.
- [53] G. Zhang, D. Choi, D. E. Kim, and J. Jung, “Reconstruction of abp networks from the ecg flow/ ppg signals using enhanced 1-d unet network,” in *2023 IEEE/ACIS*

*23rd International Conference on Computer and Information Science (ICIS)*, pp. 31–36, 2023.

- [54] E. O'Brien, J. Petrie, W. Littler, M. de Swiet, P. L. Padfield, D. G. Altman, M. Bland, A. Coats, and N. Atkins, "The british hypertension society protocol for the evaluation of blood pressure measuring devices," *Journal of Hypertension*, 1993. Background: With the increasing marketing of automated and semi-automated devices for the measurement of blood pressure, there is a need for potential purchasers to be able to satisfy themselves that such devices have been evaluated according to agreed criteria. The British Hypertension Society (BHS) published a protocol of 'requirements for the evaluation of blood pressure measuring devices with special reference to ambulatory devices in 1990. This protocol has been used to evaluate a variety of blood pressure measuring devices, including eight ambulatory devices, and comments have been received from many interested parties.
- [55] Y. Chu, K. Tang, Y.-C. Hsu, T. Huang, D. Wang, W. Li, S. I. Savitz, X. Jiang, and S. Shams, "Non-invasive arterial blood pressure measurement and spo(2) estimation using ppg signal: a deep learning framework," *BMC Medical Informatics and Decision Making*, vol. 23, no. 1, p. 131, 2023.
- [56] M. H. Sherebrin and R. Z. Sherebrin, "Frequency analysis of the peripheral pulse wave detected in the finger with a photoplethysmograph," *IEEE Transactions on Bio-medical Engineering*, vol. 37, pp. 313–7, Mar 1990.
- [57] M. Elgendi, R. Fletcher, Y. Liang, N. Howard, N. H. Lovell, D. Abbott, K. Lim, and R. Ward, "The use of photoplethysmography for assessing hypertension," *npj Digital Medicine*, vol. 2, no. 1, p. 60, 2019.
- [58] Y. Liang, M. Elgendi, Z. Chen, and R. Ward, "An optimal filter for short photoplethysmogram signals," *Scientific Data*, vol. 5, no. 1, p. 180076, 2018.
- [59] rtadmin, "Are blood pressure changes throughout the day normal?." Good Neighbor Pharmacy, Feb 2023. Available online: <https://www.mygnp.com/blog/are-blood-pressure-changes-throughout-the-day-normal/> (accessed January 14, 2024).
- [60] M. Elgendi, "Optimal signal quality index for photoplethysmogram signals," *Bioengineering*, vol. 3, no. 4, p. 21, 2016.
- [61] S. Krishnan, *Advanced analysis of biomedical signals*, pp. 157–222. Jan 2021.
- [62] S. Foundation, "How sleep apnea affects blood pressure," February 2021.
- [63] I. Perez-Pozuelo, M. Posa, D. Spathis, K. Westgate, N. Wareham, C. Mascolo, S. Brage, and J. Palotti, "Detecting sleep outside the clinic using wearable heart rate devices," *Scientific Reports*, vol. 12, no. 1, p. 7956, 2022.
- [64] P. Charlton, D. Birrenkott, T. Bonnici, M. Pimentel, A. Johnson, J. Alastruey, L. Tarassenko, P. Watkinson, R. Beale, and D. Clifton, "Breathing rate estimation from the electrocardiogram and photoplethysmogram: A review," *IEEE Reviews in Biomedical Engineering*, vol. PP, pp. 1–1, 10 2017.